Published for the International Glaciological Society

THIS MANUSCRIPT HAS BEEN SUBMITTED TO THE JOURNAL OF GLACIOLOGY AND HAS NOT BEEN PEER-REVIEWED.

Modelling lateral meltwater flow and superimposed ice formation atop Greenland's near-surface ice slabs

Journal:	*Journal of Glaciology*
Manuscript ID	Draft
Manuscript Type:	Article
Date Submitted by the Author:	n/a

Complete List of Authors:	Clerx, Nicole; University of Fribourg, Geoscience Machguth, Horst; University of Fribourg Department of Geosciences, Department of Geosciences Tedstone, Andrew; University of Fribourg, Department of Geosciences Van As, Dirk; GEUS, Glaciology and Climate

Keywords:	Glacier hydrology, Glaciological model experiments, Melt - surface, Snow/ice surface processes

Abstract:	At high elevations on the Greenland ice sheet meltwater percolates and refreezes in place, and hence does not contribute to mass loss. However, meltwater generation and associated surface runoff is occurring from increasingly higher altitudes, causing changes in firn stratigraphy that have led to the presence of near-surface ice slabs. These ice slabs force meltwater to flow laterally instead of percolating downwards. Here we present a simple, physics-based quasi 2D-model to simulate lateral meltwater runoff and superimposed ice formation on top of ice slabs. Using a Eulerian Darcy flow scheme, the model calculates how far meltwater can travel within a melt season and when it appears at the snow surface. Results show that lateral flow is a highly efficient mechanism for runoff, as in any model grid cell lateral outflow is over 30 times larger than the amount of meltwater generated in situ. Superimposed ice formation can retain up to 40% of the available meltwater, and delays visible runoff. Validating the model against field or remote sensing data remains challenging, but the results presented here

	are a first step towards a more comprehensive understanding and description of the hydrological system in the accumulation zone of the southwestern Greenland ice sheet.

Journal of Glaciology, Vol. , No. , 1

Modelling lateral meltwater flow and superimposed ice formation atop Greenland's near-surface ice slabs

Nicole Clerx,[1] Horst Machguth,[1] Andrew J. Tedstone,[1] Dirk van As[2]

[1]*Department of Geoscience, University of Fribourg, Fribourg, Switzerland*

[2]*Geological Survey of Denmark and Greenland (GEUS), Copenhagen, Denmark*

Correspondence: Nicole Clerx <nicole.clerx@unifr.ch>

ABSTRACT. At high elevations on the Greenland ice sheet meltwater percolates and refreezes in place, and hence does not contribute to mass loss. However, meltwater generation and associated surface runoff is occurring from increasingly higher altitudes, causing changes in firn stratigraphy that have led to the presence of near-surface ice slabs. These ice slabs force meltwater to flow laterally instead of percolating downwards. Here we present a simple, physics-based quasi 2D-model to simulate lateral meltwater runoff and superimposed ice formation on top of ice slabs. Using a Eulerian Darcy flow scheme, the model calculates how far meltwater can travel within a melt season and when it appears at the snow surface. Results show that lateral flow is a highly efficient mechanism for runoff, as in any model grid cell lateral outflow is over 30 times larger than the amount of meltwater generated in situ. Superimposed ice formation can retain up to 40% of the available meltwater, and generally delays visible runoff. Validating the model against field or remote sensing data remains challenging, but the results presented here are a first step towards a more comprehensive understanding and description of the hydrological system in the accumulation zone of the southwestern Greenland ice sheet.

INTRODUCTION

The Greenland ice sheet is losing mass at an accelerating rate, and since around the year 2000 the surface mass balance has become the dominant driver of ice sheet mass loss (van den Broeke and others, 2016; Bamber and others, 2018; the IMBIE Team, 2019). Increasing summer meltwater generation and associated runoff is the main driver of the declining surface mass balance, in particular in the southwestern part of the Greenland ice sheet (Nienow and others, 2017; van den Broeke and others, 2017; Mouginot and others, 2019). From 1996 onwards, there has been a clear acceleration in meltwater runoff and discharge (Enderlin and others, 2014; van den Broeke and others, 2016).

This increase in runoff coincides with an expansion of the area in which mass loss occurs: as a result of higher summer temperatures, positive feedback mechanisms and record melt events, surface melt and runoff have increasingly occurred from higher elevations in recent years (Hanna and others, 2008; Nghiem and others, 2012; van As and others, 2012; McGrath and others, 2013; Ahlstrøm and others, 2017). In this context, we distinguish between the runoff limit and the visible runoff limit. The runoff limit is the highest elevation from which part of the locally generated meltwater flows towards the ice sheet margin, i.e. where meltwater input exceeds the retention capacity of snow and firn (e.g. Pfeffer and others, 1991; Reeh, 1991; Braithwaite and others, 1994). Above the runoff limit all meltwater refreezes locally and does not contribute to mass loss; the runoff limit location and its migration throughout the melt season therefore plays an important role in the ice sheet surface mass balance (van As and others, 2016; Nienow and others, 2017). We define the visible runoff limit as the uppermost altitude at which liquid meltwater is visible at the surface and drains through surface streams and river networks, similar to Müller (1962).

Since 2010, a series of extraordinarily warm summers have occurred. In 2010, 2012 and 2019 surface melt covered nearly all of the ice sheet (Box and others, 2011; Nghiem and others, 2012; Tedesco and Fettweis, 2020). Melting at high elevation causes structural changes in snow and firn, partly by settling upon first wetting and snow grain metamorphosis (Marshall and others, 1999), but also by refreezing of meltwater forming infiltration ice bodies such as ice glands, lenses and layers within the snow and firn (Benson, 1996).

Ice sheet-wide, between 1985 and 2020, the maximum visible runoff limit rose by on average 194 metres, expanding the visible runoff area by around 29% (Tedstone and Machguth, 2022). This observed rise in the visible runoff limit may be attributed to changes in firn stratigraphy caused by the intensive meltwater refreezing following extreme melt summers. These events have led to the formation of thick ice layers, also called ice slabs, which have been identified in firn cores and through airborne radar data since 2010 (Machguth and others, 2016; MacFerrin and others, 2019). These ice slabs act as aquitards, forcing meltwater to runoff laterally rather than allowing it to percolate to depth. Recent studies furthermore show that significant melt events directly impact the occurrence, distribution and thickness of near-surface ice slabs (Culberg and others, 2021; Jullien and others, 2023).

Under melting conditions, slush fields develop on top of near-surface ice slabs at different elevations in the accumulation zone of the southwestern Greenland ice sheet. Slush fields are water-saturated areas of snow and firn with visible meltwater ponding on the surface, and constitute an important component in the hydrological system strongly linked to runoff (Holmes, 1955). Field observations show that meltwater flows laterally through the slush matrix before fully saturating the snowpack and causing slush fields to become visible on the ice sheet surface (Clerx and others, 2022). The prerequisites for the transition from vertical water percolation to lateral meltwater flow, as well as the exact processes driving the evolution of slush fields between their first appearance to subsequent drainage, however, remain unclear.

A common approach for modelling meltwater flow through snow and firn is the "tipping bucket" scheme, where the firn is vertically divided into layers and after exceeding a set threshold value for water saturation, water moves between model layers instantaneously. Once reaching the bottommost grid cell in the vertical domain or another impermeable grid cell, instantaneous runoff takes place hence mimicking lateral meltwater flow. Bucket schemes are applied in the main regional climate models (RCMs) used for predicting the Greenland ice sheet mass balance, the Regional Atmospheric Climate Model (RACMO; Noël and others, 2019), the Modèle Atmosphérique Régional (MAR; Fettweis and others, 2017) and HIRHAM (Bøssing Christensen and others, 2007). In RACMO, the bucket scheme is enhanced by its coupling to a simplified version of the IMAU-FDM (Firn Densification Model) to simulate changes in firn properties and meltwater percolation (Ligtenberg and others, 2011; Kuipers Munneke and others, 2014, 2015; Noël and others, 2018). The HIRHAM model, an RCM developed by the Danish Meteorological Institute and the Alfred Wegener Institute Foundation for Polar and Marine Research, also uses an enhanced bucket scheme to approximate lateral meltwater runoff (Langen and others, 2017). Here, water in excess of the irreducible water saturation runs off only after a certain characteristic residence time τ_{RO} that is related to local slope (Zuo and Oerlemans, 1996). Another, more physics-based approach for water flow through snow employs the Richards equation, and is used in models like SNOWPACK (Bartelt and Lehning, 2002; Lehning and others, 2002) or for example the continuum model by Meyer and Hewitt (2017). The disadvantage of these more complicated models is their computation time, which makes integration with already CPU-heavy RCMs unrealistic. All of the models mentioned here operate along a vertical axis only, and hence do not explicitly model lateral meltwater flow.

For capturing lateral liquid water transport in the snowpack on a multi-km scale the tipping bucket approximation is robust and useful, as simplified models have been shown to provide runoff predictions that closely match those of significantly more complex snow-physics models (Magnusson and others, 2015). However, existing parametrisations for meltwater processes, and estimates of refreezing and retention in the surface mass balance simulated by regional climate models (RCMs) remain major contributors to the total uncertainty in future mass balance predictions (Smith and others, 2017; Nienow and others, 2017). This uncertainty is highlighted when comparing the surface runoff area modelled by two RCMs to satellite-based observations: the RCMs overestimate the surface runoff area by 16-30% (Tedstone and Machguth, 2022). Vandecrux and others (2020) evaluated nine different firn models in the retention model intercomparison project RetMIP, and found that the model spread in meltwater retention and runoff quantities increases with increasing meltwater input. Refreezing could account for retention of up to almost half (40-46%) of the total amount of liquid water input on the Greenland ice sheet, although this estimate remains highly ambiguous given the lack of understanding of the importance of specific hydrological processes in firn (Steger and others, 2017). These findings emphasize the significant uncertainty regarding the fate of meltwater, especially when considering future ice sheet mass balance scenarios in a warming climate.

Improving estimates of total runoff from RCMs requires more knowledge of the hydrological processes at and around the runoff limit. Furthermore, this increased understanding of meltwater hydrology should be more effectively integrated into RCMs. In mountain hydrology, numerous sophisticated (2D) models exist that route water through different reservoirs in a hydrological catchment and couple surface- and subsurface flow, like for example the mesoscale Hydrological Model (mHM; Samaniego and others, 2010; Kumar and others, 2013), the ParFlow-Community Land Model (Maxwell and Miller, 2005; Kollet and Maxwell, 2006) and MODFLOW (McDonald and Harbaugh, 1988; Harbaugh and others, 2000). However, initialisation and calibration of these models often requires a lot of (small-scale) field observations, and the complex calculations in these models prohibit a thorough interpretation of results. A conceptual 2D-model for perennial firn aquifers using the modified ground water model SUTRA-ICE was recently published (Miller and others, 2022), but this model is not suitable in scenarios where near-surface ice slabs play an important role in the hydrological system. This limitation arises primarily from its use of a fixed, constant snow depth, which fails to accurately represent cases where surface lowering due to melt plays an important role, such as when the snowpack on top of the ice slab is relatively thin.

In this paper we present a quasi 2D-model of runoff, that simulates lateral meltwater flow and refreezing on top of an ice slab on the southwest Greenland ice sheet. In our simple, low-CPU-intensive model we use a Eulerian Darcy flow scheme to calculate (i) the distance meltwater can travel before fully saturating the snowpack and hence becoming visible at the snow surface within a melt season, and (ii) when this meltwater breakthrough at the surface (i.e. slush formation) occurs. The ultimate goal of the model is to reproduce the evolution of water table height throughout the melt season, to investigate the total amount of meltwater present between the visible and actual runoff limits. This would help quantify the amount of water available for either runoff or refreezing thereby contributing to the further thickening of near-surface ice slabs. Here we introduce the model concept, and establish which parameters influence the timing and location of the visible runoff appearance.

STUDY AREA AND CLIMATOLOGICAL SETTING

Our study region is the southwest of the Greenland ice sheet around 67°N, 47°W near the upper end of the K-transect (van de Wal and others, 2005, 2012). Ice slabs have been identified at elevations up to 1900 m a.s.l. here (Machguth and others, 2016; Jullien and others, 2023) and the maximum annual visible runoff limit since 2012 ranges from 1650-∼1840 m a.s.l. (Tedstone and Machguth, 2022; Machguth and others, 2022). Extensive meteorological data is available from the nearby PROMICE weather stations, of which KAN_M and KAN_U, at respectively 1270 and 1840 m a.s.l., are the two most relevant for the area of interest (Ahlstrøm and others, 2008; How and others, 2022).

Since 2010, average winter accumulation in the study area was approximately 0.3–0.4 m w.e. (e.g. Ahlstrøm and others, 2017; Smeets and others, 2018; How and others, 2022), and the site is gradually becoming closer and closer to the migrating equilibrium line. In the period from 1990–2011 the average equilibrium line altitude (ELA) was at 1553 m a.s.l. (van de Wal and others, 2012). The mean annual air temperature for the years 2008 to 2020 was -14.8 $^{\circ}$C (Fausto and others, 2021), and in the period from 2011 to 2021 the melt season counted between 12 and 47 positive degree days (Xiao and others, 2022). Average surface slope between 1900 and 1700 m a.s.l. in the study area is -0.005, equivalent to an elevation loss of approximately 5 m over 1 km according to the ArcticDEM (Porter and others, 2018).

METHODS

Our model is based on Darcy's law for flow through a porous medium. It consists of a downslope transect of grid cells where each grid cell has a fixed initial height and is made up of isothermal dry snow at 0◦C at the start of every model run. Each grid cell is divided into two domains: vertical percolation and lateral flow. If melt occurs, the model checks whether the snowpack is saturated using a fixed irreducible water saturation threshold, and if so, determines the amount of meltwater that percolates into the lateral flow domain. Subsequently, it calculates the lateral flow of meltwater based on the hydraulic gradient between adjacent grid cells. Vertical meltwater percolation is assumed to occur "instantaneously", i.e. water that has percolated vertically can be transported laterally within the same timestep. The grid cell height either remains constant, or, when surface lowering due to melt is applied, decreases by the amount of melt in a specific grid cell at each timestep. If refreezing is employed, the amount of superimposed ice formation is determined every timestep and this is also subtracted from the water table- and grid cell height. Refreezing only takes place at the bottom of each cell, in the form of ice accreting on top of the underlying ice slab.

Figure 1 shows a schematic of the lateral flow model. The bottom of all grid cells is a no-flow boundary for meltwater with, in case of refreezing, a negative conductive heat flux. No lateral inflow can take place in the uppermost grid cell, because we assume this is the location of the actual runoff limit. The outflow of the bottommost grid cell along the transect is calculated based on the hydraulic gradient of the second-to-last grid cell, to avoid any artificial accumulation or accelerated drainage of meltwater at the end of the transect. As soon as the water level equals the grid cell height in any one of the grid cells along the modelled transect (i.e. once the vertical percolation domain does not exist anymore) the simulation is stopped, as surface runoff is not currently included in the model. Total discharge is the amount of water having flowed out of the bottommost grid cell of the modelled transect.

We simulate various model scenarios, based on four melt summers (April 1st–October 1st for two warmer and two colder melt seasons), two slope types (a constant slope for sensitivity testing, and the K-transect slope for more data-based simulations), three elevation ranges (1900-1700, 1900-1800 and 1800-1700 m a.s.l.), and finally including and excluding surface lowering by melt and refreezing/superimposed ice formation. The underlying philosophy is to encompass a range of scenarios, spanning from highly conceptual setups for model- and sensitivity testing to more empirically driven model runs, allowing for qualitative comparison with field observations.

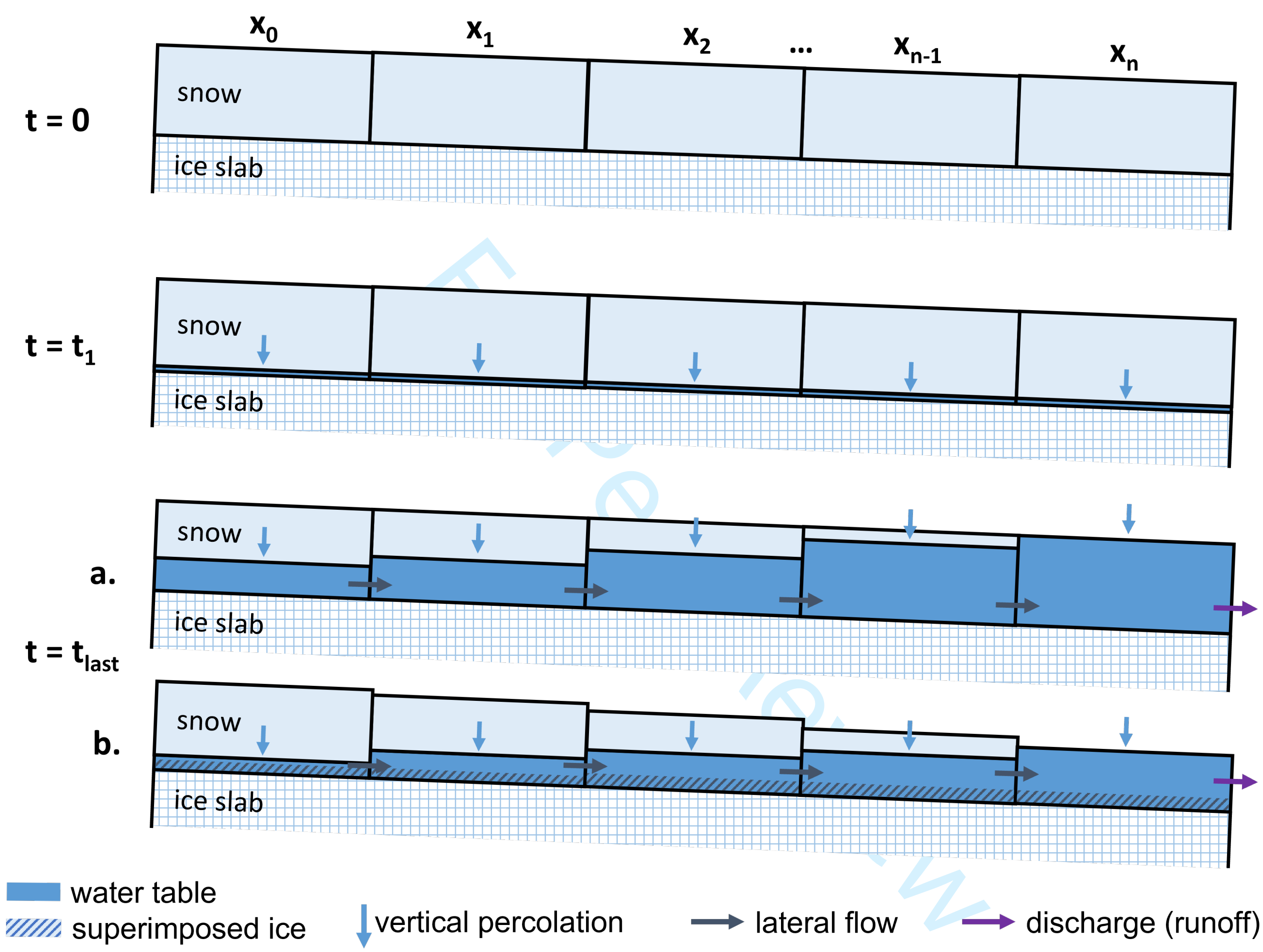

Fig. 1. Model schematic at three different time steps. For t=t_0 and t=t_1 no visible differences are present between the various modelling scenarios (t_1 being the first timestep in which melt occurs). For t=t_{last} the two most extreme cases are displayed: (a) without surface lowering and refreezing, and (b) with surface lowering and superimposed ice formation.

Table 1. Values of the parameters used in this study

Description		Value	Units
General			
Gravity constant	g	9.81	m s^{-2}
Ice density at -10◦C	ρ_i	918.9	kg m^{-3}
Fluid density of water at 0◦C	ρ_w	1000	kg m^{-3}
Dynamic viscosity of water	μ	$1.7916 \cdot 10^{-3}$	Pa·s
Snowpack porosity	ϕ	0.45	-
Meltwater flow			
Vertical percolation velocity	k_{vertical}	$6.94 \cdot 10^{-5}$	m s^{-1}
Lateral flow velocity	k_{lateral}	$1.92 \cdot 10^{-3}$	m s^{-1}
Irreducible water saturation	$S_{\mathrm{w,irr}}$	0.01	-
Hydraulic conductivity	K	0.384	m s^{-1}
Refreezing			
Heat capacity of ice	c_p	$2.0 \cdot 10^3$	J kg^{-1} K^{-1}
Thermal conductivity of ice	K_{therm}	2.30	W m^{-1} K^{-1}
Latent heat of freezing	L	$3.34 \cdot 10^5$	J kg^{-1}
Ice slab surface temperature at 0 m depth	T_{slush}	0	◦C
Ice slab temperature at 2-10 m depth	T_{iceslab}	-10	◦C
Model properties			
Average ice slab surface slope		-0.005	m m^{-1}
Initial snowpack height	h	0.5 or 1.0	m w.e.
Grid cell width	dx	100	m
Transect length	L	13.6 to 28.6	km
Timestep	dt	3600	s

Required inputs for the model include transect slope, grid cell width and initial snow height, snow/firn hydrological properties (porosity, hydraulic conductivity and irreducible water saturation), initial ice slab temperature gradient and meltwater input over time. For the slope of the grid cell transect, we either use an averaged, continuously downhill slope equal to the average K-transect slope between 1900 and 1700 m a.s.l. or the actual slope along the K-transect according to the ArcticDEM (Porter and others, 2018) in the defined elevation range. Model transects have a length of 13 to 29 km depending on which elevation range is used, all with a constant grid cell width of 100 m. The initial grid cell height or snowpack thickness is set to either 1 m w.e. for the conceptual model runs with a constant slope, or reduced to 0.5 m w.e. for the more empirical simulations to represent the relatively low amount of winter accumulation in this area. We use an average porosity of 45% following the field measurements described in Clerx and others (2022), and divide their observed lateral meltwater flow velocity ($1.92 \cdot 10^{-1}$ m s^{-1}) by the local surface slope from the ArcticDEM (-0.005, or ∼5 m elevation loss over 1 km) as hydraulic gradient to obtain the slush hydraulic conductivity (0.384 m s^{-1}). Irreducible water saturation is set to 2%, which is the lower bound of $S_{w,irr}$ observed in the long-term drainage experiments in snow and firn by Denoth (1982). All values for the parameters of the different model components are given in Table 1.

Variables calculated every timestep include snowpack height (thickness of the vertical percolation domain), water table height (thickness of the lateral flow domain), the volume of water flowing into and out of both model domains, the amount superimposed ice formation and the resulting hydraulic gradient. All output is given in m w.e. To ensure model stability, a sufficiently small timestep needs to be chosen such that the vertical percolation distance is always smaller than the defined grid cell height, and the lateral distance meltwater can flow in one timestep is always less than the grid cell width. For our simulations, hourly timesteps were chosen, resolving the daily cycle.

Meltwater flow

Darcy's law is an empirical equation describing the flow of a fluid through a porous medium. It relates the flow rate of the fluid to the hydraulic gradient:

$$q = \frac{Q}{A} = -K\frac{dh}{dx} \tag{1}$$

where q is the specific discharge, sometimes also called Darcy velocity [m s^{-1}], Q is the flow rate or total discharge [m^3 s^{-1}], $\frac{dh}{dx}$ is the hydraulic gradient [m m^{-1}], A is the area through which flow occurs [m^2] and

K the hydraulic conductivity [m s^{-1}].

The hydraulic head h is a measure of fluid potential, or otherwise said the liquid pressure above a certain datum. It is the sum of two components: the elevation head z and the pressure head Ψ. Given that we are dealing with a single fluid, water, in an unpressurised system (where grid cells are open to the atmosphere), the pressure head is constant everywhere and the fluid potential is solely a result of the water table height and topographical elevation. Consequently, the hydraulic head can be simplified to the elevation head z. The hydraulic gradient is the difference in hydraulic head over the length of the flow path, which in this case is the distance between adjacent grid cells.

The hydraulic conductivity K describes the ease with which a fluid can move through a porous medium. It depends on the intrinsic permeability of the medium, the degree of fluid saturation and on the density and viscosity of the fluid, and is defined as:

$$K = \frac{k\rho g}{\mu} \tag{2}$$

with k being the matrix permeability [m^2], and ρ and μ the density [kg m^{-3}] and dynamic viscosity of the fluid [Pa·s]. Permeability is a medium-specific quantity that is not influenced by the fluid properties.

Meltwater input

Meltwater input for the simulations was obtained from the surface energy balance model (SEBM) described in van As (2011); van As and others (2012, 2017). This SEBM uses interpolated data from the weather stations along the K-transect and calibrated satellite-derived albedo data in an observation-based approach to calculate all surface mass- and energy fluxes in 100 m-surface elevation bins. Liquid water supplied to the snowpack by rainfall or condensation is assumed negligible and not included in our model runs.

To investigate the impact of varying melt season characteristics, we selected four years with distinctly different melt patterns: 2012 and 2019, classified as "warm" or "high-melt" years, and 2017 and 2020, categorized as "cold" or "low-melt" years. Apart from variations in the total supplied meltwater for each year, all years show a distinct temporal evolution of the melt season. Figure 2 illustrates these differences. In 2012, early melt peaks were observed in June, whereas 2019 featured a later and more gradual development of meltwater supply. Likewise, in 2020 there was a major melt event mid-late August, in contrast to 2017 according to the SEBM. Note that the total cumulative melt along the K-transect in 2019 is relatively low compared to 2012, but according to GRACE and other mass balance measurements it was a large mass loss-year Greenland-wide (Tedesco and Fettweis, 2020). Furthermore, the maximum elevation of the visible

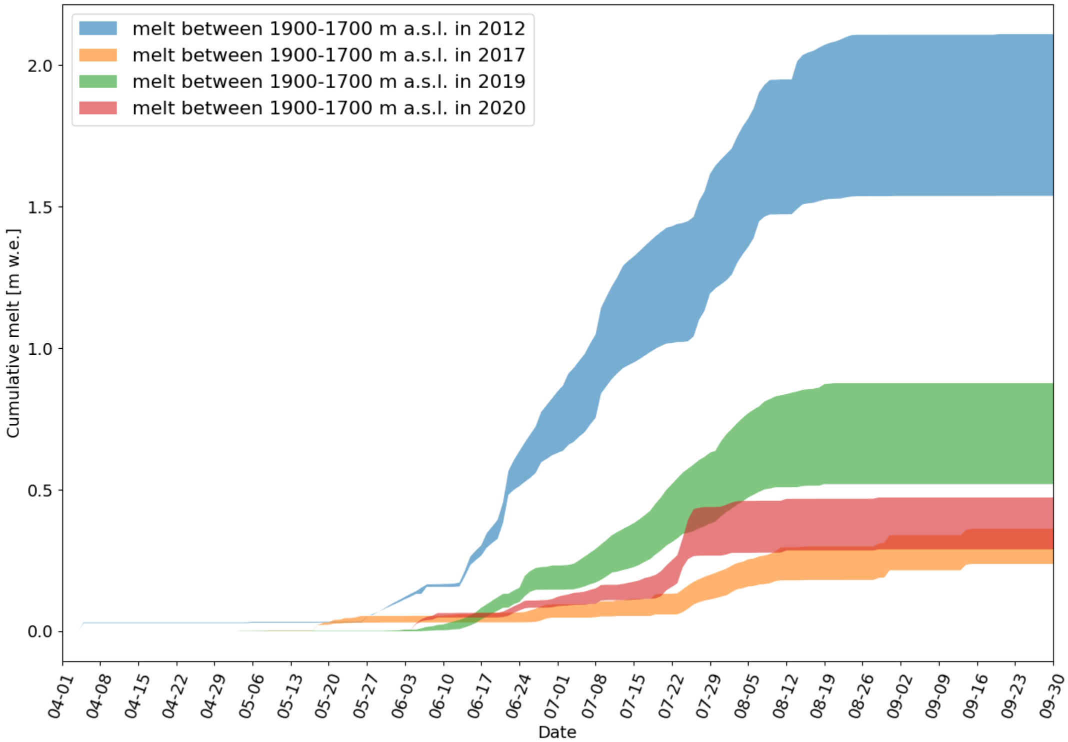

Fig. 2. Cumulative melt over time for the four melt seasons at 1800 m a.s.l. along the K-transect (67○N, 47○W) used as input for simulations.

runoff limit in 2019 (1822 m a.s.l.) was comparable to the the record year of 2012 (1841 m a.s.l.). In 2017 and 2020 the visible runoff limit was identified at lower altitudes, at 1663 and 1708 m a.s.l. respectively (Machguth and others, 2022).

Refreezing

Refreezing is the freezing of liquid water delivered to the glacier surface (i.e. meltwater generated in situ, or rain) having percolated to some depth (Cogley and others, 2011). Meltwater infiltration and refreezing processes are dependent on the timing and quantity of meltwater input and initial temperature conditions (Pfeffer and Humphrey, 1998). Cogley and others (2011) specify that "when refreezing occurs below the previous summer's surface it represents internal accumulation, when it occurs at the base of snow overlying impermeable glacier ice it is called superimposed ice" (SI). However, since summer surfaces are hard to reliably locate in the accumulation zone of the Greenland ice sheet and are not relevant in our minimalistic model approach, we consider all refreezing to result in superimposed ice and do not distinguish between SI formation and internal accumulation. Our definition of superimposed ice hence bears more resemblance to the term infiltration ice, meaning ice derived from the refreezing of meltwater having filled up snow- or firn porosity (Shumskii, 1964).

In our model an isothermal snow layer overlies the ice slab which initially has a subfreezing temperature. Meltwater which is present on top of the ice slab refreezes onto the slab based on the 1D heat equation:

$$\frac{\partial T}{\partial t} = \frac{K_{therm}}{\rho c_p} \frac{\partial^2 T}{\partial z^2} \tag{3}$$

where T is the ice slab temperature [◦C], ρ the ice slab density [kg m^{-3}] and c_p the specific heat capacity of ice at -10◦C [J kg^{-1} K^{-1}]. The temperature change $\frac{\partial T}{\partial t}$ [◦C s^{-1}] determines the amount of refreezing Δz [m w.e.] that can take place in each time step following:

$$\Delta z = \frac{1}{L}\left(\frac{\partial T}{\partial t} * \Delta t\right) \tag{4}$$

with L the latent heat of freezing [J kg^{-1}] and Δt the timestep length [s].

We calculate the negative heat flux generated by the ice slab and the resulting amount of refreezing at the ice slab surface using a forward Euler-scheme, assuming an ice slab thickness of 10 m. We use an initial ice slab temperature gradient extending from 0 to 2 m where the temperature linearly decreases from 0◦C at the surface to -10◦C at 2 m depth. Below this point, the ice slab initially has a constant temperature of -10◦C to 10 m depth. This configuration was chosen to broadly represent temperature profiles as measured in situ, particularly around the time when the snowpack becomes isothermal due to melting and vertical percolation. Throughout the simulation, the heat flux, and hence the refreezing rate, gradually decreases as the ice slab warms up.

If refreezing occurs in a model run, the amount of refrozen water is determined every timestep based on the total time passed since initial refreezing and the quantity of liquid water available. The refrozen water is subsequently subtracted from the water table and grid cell height before continuing to the next timestep.

RESULTS

Simulations along a linear slope

Figure 3 shows the evolution of water table height (a and b), snowpack thickness (c) and superimposed ice formation (d) during the 2020 melt season along a transect from 1900-1700 m a.s.l. with a linear slope, ∼29 km in length. Panels (a) and (b) illustrate that the maximum water table height reached during the summer of 2020 was determined principally by the amount of melt input, and that surface lowering and superimposed ice formation play a minor role. Surface lowering is therefore not of major interest when discussing the results for this year. When comparing panels (a) and (b), two effects of superimposed ice formation are visible. Firstly, SI formation leads to a reduction in the maximum water table height (0.41 vs. 0.35 m w.e. early August), and secondly it curtails the build-up of a water table at higher elevations, resulting in a diminished volume of liquid water present at the end of the melt season (maximum water table height of 0.33 vs. 0.23 m w.e. end September). Moreover, the water table persists further downslope at the end of the melt season when SI formation occurs, indicated by the presence of water from about 15 km along the transect onwards in (b), whereas the water table is present below around 13 km in (a) at the end of September.

Table 2 shows characteristics of the simulation results for all of the four selected melt seasons, along the same transect as used for Fig. 3. We computed normalised discharge and superimposed ice volume as fractions of the total available meltwater in each model run at the end of the simulation. Given that some simulations do not run until the end of the simulation period (1 October) because the slush limit appears throughout the melt season, the absolute volume of meltwater discharge or water retained as superimposed ice cannot be compared quantitatively.

Results show that water surfaced early in the season for 2012 and in two out of three cases for 2019, as a result of the high amount of meltwater input in these years. Although the total cumulative melt in 2019 was less than 1 m w.e., the visible runoff limit appeared around end July. In 2012 this amount of melt was already reached before mid July (see also Fig. 2), accompanied by meltwater appearing at the surface before the end of June.

The earlier in the melt season the water breakthrough, the more water is still present in the system at the end of the model run, due to the fact that there has been less time for evacuating water. This is shown by the lower values for normalised discharge in 2012 than in 2019 when looking at cases without SI-

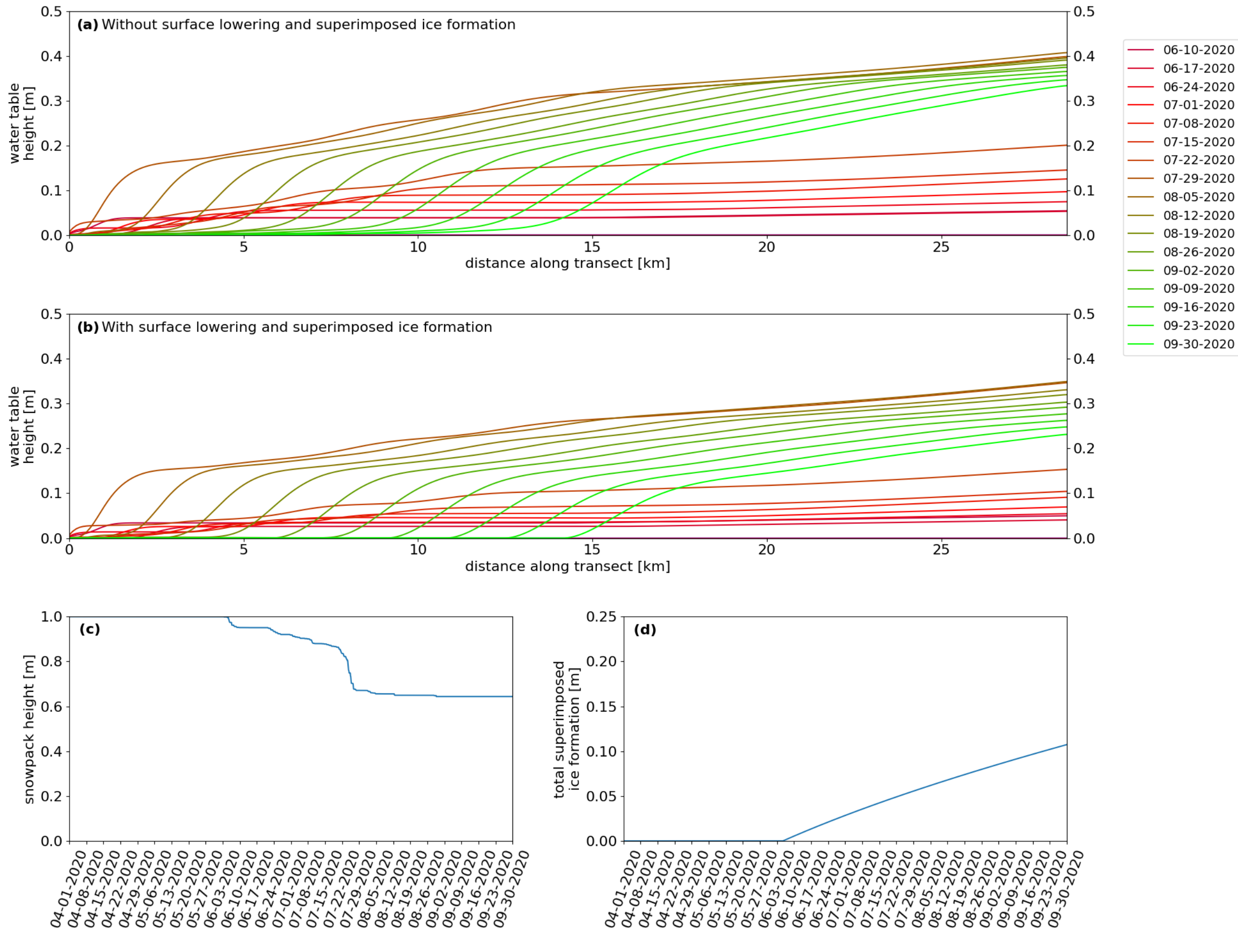

Fig. 3. Water table evolution for the 2020 model runs (a) excluding and (b) including surface lowering and superimposed ice formation. Every coloured line represents the water table height at a weekly interval after the initial occurrence of water in the lateral flow domain. For the latter scenario snowpack height (c) and cumulative superimposed ice formation (d) are shown for a grid cell in the middle of the transect.

Table 2. Simulation results for modelling runs along a transect with a constant slope between 1900 and 1700 m a.s.l. for four different melt seasons. SL and SI stand for surface lowering (due to melt) and superimposed ice formation, respectively

year	SL	SI	water break-through date	maximum water table height [m]	thickness of SI formed [m]	total normalised discharge [m^3 m^{-3}]	total normalised SI volume [m^3 m^{-3}]
2012	no	no	July 9	1.00	-	17%	-
2012	yes	no	June 22	0.50	-	10%	-
2012	yes	yes	June 22	0.47	0.06	6%	11%
2017	no	no	-	0.26	-	55%	-
2017	yes	no	-	0.26	-	55%	-
2017	yes	yes	-	0.17	0.13	32%	48%
2019	no	no	-	0.76	-	67%	-
2019	yes	no	July 23	0.48	-	19%	-
2019	yes	yes	July 24	0.46	0.05	16%	11%
2020	no	no	-	0.41	-	68%	-
2020	yes	no	-	0.41	-	68%	-
2020	yes	yes	-	0.35	0.11	53%	27%

formation. Much of this water presumably continues to drain out of the slush and into river channels which incise headwards after meltwater breakthrough, but simulating surface meltwater runoff is not included in the current modelling scope.

Surface lowering has a stronger effect on the occurrence of the visible runoff limit than superimposed ice formation: the amounts of SI formed are an order of magnitude smaller than the surface height reduction by melt (e.g. 0.05 vs. 0.5 m w.e. for 2019). SI formation, however, can reduce the total amount of runoff by up to almost half: normalised discharge is reduced to 6% with SI-formation vs. 10% without meltwater retention by superimposed ice in 2012.

Data-based scenarios: simulations with the K-transect slope

Figure 4 shows the water table height (solid lines) and snowpack thickness (dashed lines) for the 2019 (warm; panel a) and 2020 (cold; panel b) melt seasons along a transect with the actual surface slope around the weather station KAN_U following the ArcticDEM, for the case where both surface lowering and SI formation were applied and with an initial snowpack thickness of 0.5 m w.e.

Changes in transect gradient have an important effect on the water table height. Both in (a) and (b) it can be seen that at 2 km, just before 9 km and around 14 and 23 km water accumulates due to a slope decrease, whereas at 9 km, 17 km and just after 20 km water is evacuated more efficiently> This is visible from a local decrease in water table height, related to an increase in slope.

Especially in 2020 (b) the effect of lateral meltwater flow is clearly visible by the downslope migration over time of the highest water table below 2 km and 22 km, where the transect slope decreases. Similarly, in 2019 (a) the water table peak around 2 km moves slightly downslope after a short pause in meltwater supply between the 1$^{\mathrm{st}}$ and 8$^{\mathrm{th}}$ of July.

Table 3 shows the results for the simulations along the same transect as Fig. 4 for all studied melt seasons, first for a transect from 1900-1700 m a.s.l. and then for a smaller, 100 m elevation range (1900-1800 m a.s.l.) to investigate the impact of less melt at higher elevations. In all these model runs the initial snowpack height was a more realistic 0.5 m w.e. as opposed to the 1 m w.e. initial snow thickness for the reference runs of the previous section. Logically, reducing the snowpack thickness to 0.5 m w.e. has a significant impact on the model run duration: the water table now reaches the surface in all model runs except for the simulation for 2017 along the 1900-1800 m a.s.l. transect.

When only looking at the upper part of the transect (1900-1800 m a.s.l.), there is 2-5% more accretion

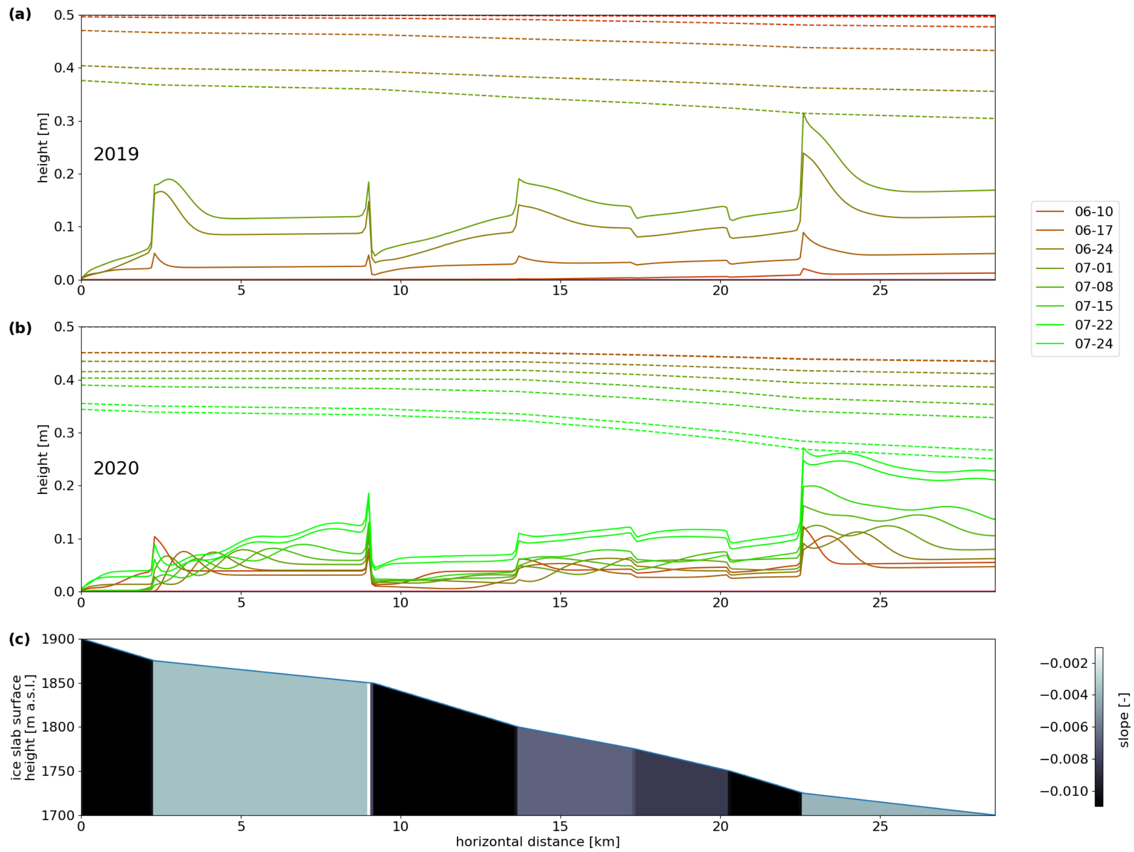

Fig. 4. Evolution of water table (solid) and snowpack (dashed) height over time for 2019 (a) and 2020 (b) with surface lowering and superimposed ice formation, and (c) grid cell height and slope gradient along the transect. Every coloured line represents a weekly interval after the initial occurrence of water in the lateral flow domain. Absent lines in 2019 (a) are a result of the simulation being stopped due to earlier water breakthrough than in 2020.

Table 3. Simulation results for modelling runs along the K-transect slope between 1900 and 1700 m a.s.l. and 1900-1800 m a.s.l. for four different melt seasons, with surface lowering due to melt and superimposed ice (SI) formation

year	water break-through date	breakthrough elevation [m a.s.l.]	maximum water table height [m]	thickness of SI formed [m]	total normalised discharge [m^3 m^{-3}]	total normalised SI volume [m^3 m^{-3}]
1900-1700 m a.s.l.						
2012	June 15	1720	0.29	0.07	4%	24%
2017	August 7	1724	0.26	0.09	10%	36%
2019	June 26	1725	0.32	0.02	3%	12%
2020	July 22	1725	0.27	0.05	11%	26%
1900-1800 m a.s.l.						
2012	June 16	1850	0.26	0.07	17%	20%
2017	-	1850	0.24	0.13	45%	40%
2019	July 12	1850	0.27	0.04	28%	14%
2020	July 24	1850	0.26	0.05	19%	21%

of superimposed ice, primarily because the model runs longer before the visible runoff limit appears. The total thickness of newly formed superimposed ice is similar across the two transect variations, though slightly thicker in the shorter 1900-1800 m a.s.l. transect.

DISCUSSION

Timing and location of slush appearance

The increase in water table height over time on top of an ice slab is dependent on the evolution of the melt season throughout the summer. Shorter, intense periods of melt are more likely to cause the appearance of visible runoff than more gradual meltwater supply, as shorter periods allow for less lateral flow through the firn evacuating the meltwater downslope.

In general, the occurrence of visible runoff takes place later in the melt season at higher elevations according to the results for the two modelled elevation intervals (Table 3): simulations using the longer 1900-1700 m a.s.l. transect result in earlier occurrence of the slush limit than on the shorter transect. This is a result of the lower amount of melt at higher elevations, as well as the impact of lateral meltwater supply. For 2012 and 2020 there is relatively little difference in timing between the two elevation ranges due to the rather abrupt, large melt events taking place towards the end of June in 2012 and late July in 2020, but for 2017 and 2019 there are significant delays in slush limit occurrence between the transect from 1900-1800 m a.s.l. when compared to 1800-1700 m a.s.l. results. Abrupt and strong melting seems to lead to flooding of the snowpack over substantial elevation intervals, whereas sustained, moderate melt does not have this effect.

In colder summers, when the water table does not reach the snow surface in the model runs, differences in the total amount of discharge and SI formed are principally due to differences in temporal evolution and the total quantity of meltwater generated during the melt season. For example, in 2017 more SI was formed because of a more gradual evolution of the melt season, whereas in 2020, when a big melt event occurred late July, a larger part of the supplied meltwater had time to run off. Apart from the higher absolute amount of liquid water available, there was less time for refreezing due to the sudden input of melt and subsequent faster lateral meltwater displacement.

When comparing the characteristics of the linear model runs (Table 2) to those of the runs with a varying slope along the K-transect (Table 3, 1900-1700 m a.s.l.), it can be seen that the influence of slope variations is larger than that of surface lowering: for the same melt input, the water table reached higher levels more rapidly when the transect followed a non-linear slope. In the simulations with a linear slope, the maximum water table attained at the end of the simulations was approximately half the initial snowpack height of 1 m w.e. In contrast, for the model runs using the K-transect slope, the maximum water table height at the time of water breakthrough exceeded the initial snowpack height in all cases ($\sim$0.6x the initial snowpack height of 0.5 m w.e.). Across all simulations, meltwater first occurred at locations characterised by a decrease in slope. This is particularly pronounced during colder summers with a gradual supply of meltwater, when lateral flow is of even greater relative importance for total runoff than when short-lived, intense melting provides the majority of liquid water. Changes in ice slab slope, or more broadly in surface slope, therefore play a major role in the occurrence of the visible runoff limit.

Our results corroborate with the findings on the daily variation of visible runoff limits by Machguth and others (2022) for the four melt seasons studied here. In particular in the simulations for the 100 m elevation transect, the timing of meltwater appearing at the surface roughly corresponds to when the maximum visible runoff limit was observed on satellite imagery. However, a comprehensive comparison with field observations remains challenging due to the simple nature of the lateral flow model. In the current model configuration, meltwater is only transported downslope, and each grid cell can only receive meltwater input from its upslope neighbour. In reality, flowpaths are a function of the surface hydrological catchment, so grid cells could receive meltwater input from more than one neighbour.

At present, simulations are stopped as soon as the water table height reaches the snow surface in any of the grid cells, since surface meltwater runoff is not included in the model. This is the most obvious (or only physically realistic) end for a model run currently. We have only very limited knowledge on how fast water flows in slush fields, or how these develop into efficient supraglacial drainage systems. From satellite imagery it is clear that, after a certain period of time with sufficient and sustained melt, slush fields nearly always transition into more confined supraglacial river systems. Given the efficiency of this process – based on remote sensing data we can observe that the development of efficient surface drainage systems is a matter of days rather than weeks, including a simplistic bucket scheme in the model for surface runoff would probably be a valid approximation. This would avoid the necessity of incorporating a full 2D-meltwater routing scheme with all related assumptions and uncertainties. Ideally, the model should always run until the end of the melt season regardless of the amount of melt to allow for adequate comparison between individual melt seasons. Including surface runoff, even in the form of a simplistic bucket scheme, would allow simulations to run for the full melt season.

Lateral meltwater runoff and hydraulic properties

Lateral meltwater runoff is highly efficient in all model simulations. For any grid cell except the uppermost along the transect, runoff greatly exceeds the amount of vertical surface meltwater input due to the large lateral inflow from higher elevations. Depending on the temporal evolution of the melt season, total lateral runoff is roughly 40 times the average meltwater input per grid cell at the time the water table reaches the snow surface. The amount of lateral runoff as a function of total melt input per grid cell is higher for the 1900-1800 m a.s.l. transect than for the transect spanning 200 m elevation (56x vs. 37x more runoff than melt input, respectively).

The model outcomes from the longer transect show lower values for the normalised discharge. This is due to approximately twice as much liquid water still being present at the end of each model run, given that the model grid is about twice as long as that of the transect spanning a 100 m elevation range.

When assessing the impact of parameter choice on the simulation results, it is crucial to consider the hydraulic conductivity values used in our model. Field measurements of hydraulic conductivity across different glaciers are fairly uniform, most likely as a result of similar firn structure characteristics due to a common rate of firn metamorphism and densification, as highlighted by Stevens and others (2018). Notably, measured firn hydraulic conductivity values at various glaciers fall within a relatively narrow range, typically between 1-5$\cdot 10^{-5}$ms^{-1} (Fountain and Walder, 1998). However, in areas where firn aquifers exist, hydraulic conductivity measurements show a considerably wider range, spanning from $2.5 \cdot 10^{-5}$ to $1.1 \cdot 10^{-3}$ms^{-1} (Miller and others, 2017), signifying substantial variability. In the southwest of Greenland hydraulic conductivity of near-surface icy firn has been measured at 2.4$\cdot 10^{-3}$ms^{-1} (Clerx and others, 2022), marking an order of magnitude increase compared to firn aquifers' hydraulic conductivity measurements (Miller and others, 2017, 2018). In our model calculations, the hydraulic conductivity parameter K ($3.84 \cdot 10^{-1}$ms^{-1}) is derived from observed lateral flow velocities of meltwater through slush, although it is not a direct material property measurement. It is worth noting that the resulting value for K is two orders of magnitude higher than those measured in laboratory-type experiments using icy firn conducted by Clerx and others (2022). When using a more theoretical approach, calculating the hydraulic conductivity of the slush matrix using the Kozeny-Carman approximation for permeability of a porous medium consisting of perfect spheres (Kozeny, 1927; Carman, 1937; Bear, 1972), with a porosity of 0.45, ρ of 1000 kg m^{-3} and μ of $1.7916 \cdot 10^{-3}$ Pa·s for water at 0◦C) yields a hydraulic conductivity of 4.40 m s^{-1}. All in all, there is a spread of multiple orders of magnitude and hence significant uncertainty in the hydraulic conductivity of snow and firn to be used in our simulations. The value currently used for K in the model is required to obtain results that resemble field measurements of lateral meltwater flow. A lower hydraulic conductivity would lead to less runoff and a delay in occurrence of the visible runoff limit.

The irreducible water saturation $S_{w,irr}$ is set to a relatively low value of 2% of the pore volume (∼0.01 of the total volume) in our simulations, to reduce the importance of the vertical flow domain in the model. We do not have detailed insights into the actual residual water saturation in slush on top of ice slabs. Furthermore, for snow much uncertainty remains in general as to what is a representative value for the irreducible water saturation. Dielectric measurements (Lemmelä, 1973) show irreducible water saturations of 0.02-0.03 for a seasonal snowpack, whereas Coléou and Lesaffre (1998) measured values for wet snow between 0.05-0.15 in a laboratory setting. We consider the lowest value for $S_{w,irr}$ as reasonable given the relatively high percolation- and lateral flow velocities compared to the model timestep, but also since large areas can undergo the transformation into slush fields within several days.

Refreezing

Superimposed ice formation can account for meltwater retention of up to 40%, especially at high elevations. In case of intermittent melt pulses this can drastically delay or even completely inhibit the occurrence of visible water at the surface. Values for total thickness of newly formed SI are slightly higher for the upper (short) K-transect model runs as melt is slightly less at higher altitudes, resulting in a somewhat larger fraction of meltwater retention.

Simulated values for superimposed ice formation on top of the ice slab (0.02-0.13 m w.e.) are in rough agreement with data from Rennermalm and others (2021) when evaluating ice slab growth at KAN_U in consecutive years. Their firn cores yield values in the order of 0.3-0.4 m accretion of ice slab thickness per year (approx. 1.6 m ice in 5 years). The lower ice accumulation in the model is presumably a result of its 1D-nature only considering meltwater inflow from one direction, whereas in reality more water can accumulate due to local ice slab topography and resulting meltwater ponding.

In the current model configuration, refreezing only takes place in the lateral flow domain. This is a simplification, as we know from literature and field observations that ice lenses and glands form in the percolation domain, but deemed appropriate given the model simplicity and purpose. Furthermore, refreezing actually also occurs from above and not only accretes SI to the top of the ice slab surface.

At the start of all the model runs on April 1st, we assume that the full snowpack on top of the ice slab is isothermal at 0$\circ$C, as we do not simulate the initial warming of the snowpack in the beginning of the melt season. Additionally, we do not model the vertical percolation domain in detail. In years characterised by low amounts of melt, this simplification does not fully capture refreezing processes, especially regarding the formation of ice lenses and intermediate refreezing that may have an impact on the flow properties of the snowpack. These assumptions hence may lead to an overestimation of SI formation in our model. However, the applied initial ice slab temperature gradient, where ice slab temperature decreases linearly from 0 to -10$\circ$C between 0-2 m depth and only remains constant at -10$\circ$C below 2 m depth, implies that a certain amount of warming has already taken place before the onset of the melt season. Field measurements of firn temperature (e.g. Humphrey and others, 2012; Machguth and others, 2016; MacFerrin and others, 2023) show that this a realistic assumption to account for and average out yearly and shorter-term variations in ice slab temperature.

In our model we do not consider snow compaction, a processes commonly accounted for in other firn models. We have chosen to exclude it here for the sake of simplicity, as on the scale of the snowpack depth, the impact of intraseasonal snow and firn densification is likely negligible, especially in the cases where surface lowering due to melt is applied.

Including refreezing in an enhanced version of the model is not straightforward due to the limited availability of field data to provide calibration. Nevertheless, such an improvement is critical, given that refreezing is a mechanism that plays a major role in ice slab formation and expansion, yet there is little research or knowledge regarding the exact quantities of water retained in this manner. Refreezing has been investigated in earlier research (e.g. Baird, 1952; Koerner, 1970; Mikhalenko, 1989; Obleitner and Lehning, 2004; Parry and others, 2007; Cox and others, 2015). However, these studies often focus solely on measuring the amount of SI formation without considering how refreezing repartitions meltwater retention vs. runoff, or they examine and simulate superimposed ice formation in isolation of lateral flow. More knowledge on the process of meltwater refreezing from the surface downwards would also be essential, to get an idea of how important this mechanism is for meltwater retention in comparison to refreezing onto the ice slab directly and to subsequently calibrate our refreezing module.

Model limitations

Our simple 1D-model simulates meltwater hydrology on top of an ice slab, and could be applied to other areas where ice slabs exist. However, in certain regions on the Greenland ice sheet, e.g. in the northwest, fractures in the ice slab increase the effective permeability enough to restrict lateral forcing of the runoff: meltwater here can still percolate into relict firn below the ice slab through surface crevasses, as identified based on radar data analysis (Culberg and others, 2022). In our study area crevasses and fractures are very rare, reducing vertical pathways, and observed hydrological features coincide with areas where the ice slabs are thicker (Jullien and others, 2023). If modelling other regions of the Greenland ice sheet, however, care should be taken that the ice slab can reliably be considered impermeable: this is an important boundary condition for the model to be applicable.

Snow accumulation throughout the melt season is currently not included in the simulations. For example, in 2020, 0.05-0.1 m w.e. of snow fell during a two-week period in July-August while carrying out the measurements described in Clerx and others (2022). Because of the minimal nature of our model, we exclude this process. More generally, measurements of summertime accumulation at specific locations (e.g. KAN_U) is available, but it is challenging to account for spatial heterogeneity of snowfall. There would be even more difficulty when also including rain, which was not measured within the study area during the four years simulated in our study. Neglecting rainfall might artificially delay the occurrence of slush at the surface since not all liquid water present is accounted for, but the amount of rainfall is guaranteed to be negligible compared to meltwater input over the entire melt season.

With the current model set-up, meltwater is only transported downslope and each grid cell can only receive water from its upslope neighbour, whereas in reality meltwater can join a flowpath from many different directions. Furthermore, in the model scenarios presented here only downslope flow takes place: all transects are either continuously downslope or have some flat areas, but no positive gradients exist along any of the model grids. In the unlikely case that the water table height in a downslope grid cell exceeds that of its upslope neighbour (due to a large difference in melt input for example), the excess water is distributed between the two grid cells and the hydraulic heads will gradually equalise. In particular refreezing would likely be more important in the case of an undulating slope (i.e. where depressions/positive gradients exist).

CONCLUSIONS

We designed a simple, physics-based 1D-model to describe lateral meltwater flow and superimposed ice formation atop near-surface ice slabs. The model was used to simulate four melt summers in the southwest of the Greenland ice sheet, and provides the development of water table- and snowpack height throughout the melt season, as well as values for the total amount of total discharge and meltwater retention in the form of newly formed superimposed ice.

Our results show that the evolution of the water table height and the occurrence or absence of a visible runoff limit is very dependent on the evolution and intensity of individual melt seasons. In general, less melt at higher altitudes leads to the later occurrence or absence of meltwater at the surface, although even in relatively colder melt seasons the water table can appear at the snow surface in case of short, intense melt events. Changes in ice slab gradient play a major role in the appearance of of the visible runoff limit.

Lateral flow is a very efficient mechanism for meltwater runoff: in any model grid cell lateral outflow is more than 30x larger than the amount of meltwater generated in situ. Measurements of snow and firn hydraulic properties exist, yet given the wide range of values provided by field observations in particular the hydraulic conductivity remains a source of uncertainty in the model. The model currently does not include any mechanism for efficient meltwater drainage at the surface once the visible runoff limit has appeared, but for further studies this should be the first major enhancement to be made.

Superimposed ice formation can account for up to 40% of meltwater retention, and especially in case of intermittent melt pulses this can drastically delay the occurrence of visible meltwater at the surface. Values of total SI formed throughout a melt season roughly match observations of ice slab thickening at KAN_U. Simplifications in the model, for example regarding the fully isothermal snowpack and the lack of internal meltwater refreezing should be considered; a better representation of the energy balance would further improve the model.

In summary, our study highlights the pivotal role of lateral flow as a mechanism driving surface meltwater runoff. However, despite the insights gained from our simplified model, direct comparison with field- or remote sensing data remains challenging. The complex nature of the hydrological processes at play makes validation of simulation results nontrivial. Efforts to enhance and expand the 1D-model are required and ongoing, but the results presented in this paper are a first step towards a more comprehensive understanding and description of the hydrological system in the accumulation zone of the southwestern Greenland ice sheet.

ACKNOWLEDGEMENTS

This study is funded by the European Research Council (ERC) under the European Union's Horizon 2020 research and innovation programme (project acronym CASSANDRA, grant agreement No. 818994). We thank Bettina Schaefli and Nander Wever for their input and advice while shaping the model design and strategy.

AUTHOR CONTRIBUTIONS

HM and NC designed the the study with contributions from AT. NC programmed the model with contributions from HM and input data provided by DvA. NC carried out the model simulations and prepared the manuscript with contributions from HM, AT and DvA.

REFERENCES

Ahlstrøm AP, Petersen D, Langen PL, Citterio M and Box JE (2008) A new programme for monitoring the mass loss of the Greenland ice sheet (doi: 10.34194/geusb.v15.5045)

Ahlstrøm AP, Petersen D, Langen PL, Citterio M and Box JE (2017) Abrupt shift in the observed runoff from the southwestern Greenland ice sheet. *Science Advances*, **3**(12) (doi: 10.1126/sciadv.1701169)

Baird PD (1952) Part I: Method of Nourishment of the Barnes Ice Cap. *Journal of Glaciology*, **2**(11), 2–9 (doi: 10.3189/S0022143000025910)

Bamber JL, Westaway RM, Marzeion B and Wouters B (2018) The land ice contribution to sea level during the satellite era. *Environmental Research Letters*, **13**(6), 1–19 (doi: 10.1088/1748-9326/aac2f0)

Bartelt P and Lehning M (2002) A physical SNOWPACK model for the swiss avalanche warning. *Cold Regions Science and Technology*, **35**(3), 123–145 (doi: 10.1016/s0165-232x(02)00074-5)

Bear J (1972) *Dynamics of fluids in porous media*. Dover Publications, ISBN 978-0-486-65675-5

Benson CS (1996) Stratigraphic studies in the snow and firn of the Greenland ice sheet. Research Report 70, U.S. Army Snow, Ice and Permafrost Research Establishment

Bøssing Christensen O, Drews M, Hesselbjerg Christensen J, Dethloff K, Ketelsen K, Hebestadt I and Rinke A (2007) The hirham regional climate model. version 5 (beta)

Box JE, A A, J C, X F, D D, T M, D v, van de Wal D, van de Wal RSW, B V and J W (2011) Greenland, in: State of the climate in 2010. *Bulletin of the American Meteorological Society* (doi: 10.1175/1520-0477-92.6.S1)

Braithwaite RJ, Laternser M and Pfeffer WT (1994) Variations of near-surface firn density in the lower accumulation area of the greenland ice sheet, pâkitsoq, west greenland. *Journal of Glaciology*, **40**(136), 477–485 (doi: 10.3189/s002214300001234x)

Carman PC (1937) Fluid flow through granular beds. *Chemical Engineering Research and Design*, **75**, S32–S48 (doi: 10.1016/s0263-8762(97)80003-2)

Clerx N, Machguth H, Tedstone A, Jullien N, Wever N, Weingartner R and Roessler O (2022) In situ measurements of meltwater flow through snow and firn in the accumulation zone of the SW greenland ice sheet. *The Cryosphere*, **16**(10), 4379–4401 (doi: 10.5194/tc-16-4379-2022)

Cogley J, Hock R, Rasmussen L, Arendt A, Bauder A, Braithwaite R, Jansson P, Kaser G, Möller M, Nicholson L and Zemp M (2011) Glossary of glacier mass balance and related terms

Coléou C and Lesaffre B (1998) Irreducible water saturation in snow: experimental results in a cold laboratory. *Annals of Glaciology*, **26**, 64–68 (doi: 10.3189/1998aog26-1-64-68)

Cox C, Humphrey N and Harper J (2015) Quantifying meltwater refreezing along a transect of sites on the Greenland icesheet. *The Cryosphere*, **9**, 691–701 (doi: 10.5194/tc-9-691-2015)

Culberg R, Schroeder DM and Chu W (2021) Extreme melt season ice layers reduce firn permeability across greenland. *Nature Communications*, **12**(1) (doi: 10.1038/s41467-021-22656-5)

Culberg R, Chu W and Schroeder DM (2022) Shallow fracture buffers high elevation runoff in northwest Greenland. *Geophysical Research Letters*, **49**(23) (doi: 10.1029/2022gl101151)

Denoth A (1982) The pendular-funicular liquid transition and snow metamorphism. *Journal of Glaciology*, **28**(99), 357–364 (doi: 10.3189/s0022143000011692)

Enderlin EM, Howat IM, Jeong S, Noh MJ, van Angelen JH and van den Broeke MR (2014) An improved mass budget for the greenland ice sheet. *Geophysical Research Letters*, **41**(3), 866–872 (doi: 10.1002/2013GL059010)

Fausto RS, van As D, Mankoff KD, Vandecrux B, Citterio M, Ahlstrøm AP, Andersen SB, Colgan W, Karlsson NB, Kjeldsen KK, Korsgaard NJ, Larsen SH, Nielsen S, Pedersen AØ, Shields CL, Solgaard AM and Box JE (2021) Programme for monitoring of the greenland ice sheet (PROMICE) automatic weather station data. *Earth System Science Data*, **13**(8), 3819–3845 (doi: 10.5194/essd-13-3819-2021)

Fettweis X, Box JE, Agosta C, Amory C, Kittel C, Lang C, van As D, Machguth H and Gallée H (2017) Reconstructions of the 1900–2015 greenland ice sheet surface mass balance using the regional climate MAR model. *The Cryosphere*, **11**(2), 1015–1033 (doi: 10.5194/tc-11-1015-2017)

Fountain AG and Walder JS (1998) Water flow through temperate glaciers. *Reviews of Geophysics*, **36**(3), 299–328 (doi: 10.1029/97rg03579)

Hanna E, Huybrechts P, Steffen K, Cappelen J, Huff R, Shuman C, Irvine-Fynn T, Wise S and Griffiths M (2008) Increased runoff from melt from the greenland ice sheet: A response to global warming. *Journal of Climate*, **21**(2), 331–341 (doi: https://doi.org/10.1175/2007JCLI1964.1)

Harbaugh AW, Banta ER, Hill MC and McDonald MG (2000) Modflow-2000, the u.s. geological survey modular ground-water model - user guide to modularization concepts and the ground-water flow process

Holmes CW (1955) Morphology and hydrology of the Mint Julep area, southwest Greenland. In *Project Mint Julep Investigation of Smooth Ice Areas of the Greenland Ice Cap, 1953; Part II Special Scientific Reports*, Arctic, Desert, Tropic Information Center; Research Studies Institute; Air University

How P, Abermann J, Ahlstrøm A, Andersen S, Box JE, Citterio M, Colgan W, Fausto R, Karlsson N, Jakobsen J, Langley K, Larsen S, Mankoff K, Pedersen A, Rutishauser A, Shield C, Solgaard A, Van As D, Vandecrux B and Wright P (2022) Promice and gc-net automated weather station data in greenland (doi: 10.22008/FK2/IW73UU)

Humphrey NF, Harper JT and Pfeffer WT (2012) Thermal tracking of meltwater retention in greenland's accumulation area. *Journal of Geophysical Research: Earth Surface*, **117**(F1), F01010 (doi: 10.1029/2011jf002083)

Jullien N, Tedstone AJ, Machguth H, Karlsson NB and Helm V (2023) Greenland ice sheet ice slab expansion and thickening. *Geophysical Research Letters*, **50**(10) (doi: 10.1029/2022gl100911)

Koerner RM (1970) Some Observations on Superimposition of Ice on the Devon Island Ice Cap, N.W.T. Canada. *Geografiska Annaler*, **52**(1), 57–67 (doi: 10.1080/04353676.1970.11879808)

Kollet SJ and Maxwell RM (2006) Integrated surface–groundwater flow modeling: A free-surface overland flow boundary condition in a parallel groundwater flow model. *Advances in Water Resources*, **29**(7), 945–958 (doi: 10.1016/j.advwatres.2005.08.006)

Kozeny J (1927) Über kapillaire leitung des wassers im boden. *Sitzungsberichte der Akademie der Wissenschaften mathematisch-naturwissenschaftliche Klasse*, **136**, 271–306

Kuipers Munneke P, Ligtenberg SRM, van den Broeke MR, van Angelen JH and Forster RR (2014) Explaining the presence of perennial liquid water bodies in the firn of the greenland ice sheet. *Geophysical Research Letters*, **41**(2), 476–483 (doi: 10.1002/2013gl058389)

Kuipers Munneke P, Ligtenberg SRM, Noël BPY, Howat IM, Box JE, Mosley-Thompson E, McConnell JR, Steffen K, Harper JT, Das SB and van den Broeke MR (2015) Elevation change of the Greenland ice sheet due to surface mass balance and firn processes, 1960–2014. *The Cryosphere*, **9**, 2009–2025

Kumar R, Samaniego L and Attinger S (2013) Implications of distributed hydrologic model parameterization on water fluxes at multiple scales and locations. *Water Resources Research*, **49**(1), 360–379 (doi: 10.1029/2012wr012195)

Langen PL, Fausto RS, Vandecrux B, Mottram RH and Box JE (2017) Liquid water flow and retention on the Greenland ice sheet in the regional climate model HIRHAM5: Local and large-scale impacts. *Frontiers in Earth Science*, **4**, 110 (doi: 10.3389/feart.2016.00110)

Lehning M, Bartelt P, Brown B, Fierz C and Satyawali P (2002) A physical SNOWPACK model for the Swiss avalanche warning Part II. snow microstructure. *Cold Regions Science and Technology*, **35**(3), 147–167 (doi: 10.1016/s0165-232x(02)00073-3)

Lemmelä R (1973) Measurements of evaporation-condensation and melting from a snowcover. In *The Role of Snow and Ice in Hydrology*

Ligtenberg SRM, Helsen MM and van den Broeke MR (2011) An improved semi-empirical model for the densification of Antarctic firn. *The Cryosphere*, **5**, 809–819 (doi: 10.5194/tc-5-809-2011)

MacFerrin M, Machguth H, van As D, Charalampidis C, Stevens CM, Heilig A, Vandecrux B, Langen PL, Mottram R, Fettweis X, van den Broeke MR, Pfeffer WT, Moussavi MS and Abdalati W (2019) Rapid expansion of greenland's low-permeability ice slabs. *Nature*, **573**(7774), 403–407 (doi: 10.1038/s41586-019-1550-3)

MacFerrin MJ, Stevens CM, Vandecrux B, Waddington ED and Abdalati W (2023) The greenland firn compaction verification and reconnaissance (FirnCover) dataset, 2013–2019. *Earth System Science Data*, **14**(2), 955–971 (doi: 10.5194/essd-14-955-2022)

Machguth H, MacFerrin M, van As D, Box JE, Charalampidis C, Colgan W, Fausto RS, Meijer HA, Mosley-Thompson E and van de Wal RS (2016) Greenland meltwater storage in firn limited by near-surface ice formation. *Nature Climate Change*, **6**, 390–393 (doi: 10.1038/nclimate2899)

Machguth H, Tedstone AJ and Mattea E (2022) Daily variations in western greenland slush limits, 2000–2021. *Journal of Glaciology*, **69**(273), 191–203 (doi: 10.1017/jog.2022.65)

Magnusson J, Wever N, Essery R, Helbig N, Winstral A and Jonas T (2015) Evaluating snow models with varying process representations for hydrological applications. *Water Resources Research*, **51**(4), 2707–2723 (doi: 10.1002/2014wr016498)

Marshall H, Conway H and Rasmussen L (1999) Snow densification during rain. *Cold Regions Science and Technology*, **30**(1-3), 35–41 (doi: 10.1016/s0165-232x(99)00011-7)

Maxwell RM and Miller NL (2005) Development of a coupled land surface and groundwater model. *Journal of Hydrometeorology*, **6**(3), 233–247 (doi: 10.1175/jhm422.1)

McDonald M and Harbaugh A (1988) A modular three-dimensional finite-difference ground-water flow model

McGrath D, Colgan W, Bayou N, Muto A and Steffen K (2013) Recent warming at summit, greenland: Global context and implications. *Geophysical Research Letters*, **40**(10), 2091–2096 (doi: 10.1002/grl.50456)

Meyer CR and Hewitt IJ (2017) A continuum model for meltwater flow through compacting snow. *The Cryosphere*, **11**, 2799–2813 (doi: 10.5194/tc-11-2799-2017)

Mikhalenko VN (1989) Osobennosti massoobmena lednikov ploskikh vershin vnutrennogo Tjan'-Shanja (Properties of mass exchange of plateau glaciers in the inner Tjan-Shan)). *Materials of glaciological studies*, **65**, 86–92

Miller O, Solomon DK, Miège C, Koenig L, Forster R, Schmerr N, Ligtenberg SRM and Montgomery L (2018) Direct evidence of meltwater flow within a firn aquifer in southeast greenland. *Geophysical Research Letters*, **45**(1), 207–215 (doi: 10.1002/2017gl075707)

Miller O, Voss CI, Solomon DK, Miège C, Forster R, Schmerr N and Montgomery L (2022) Hydrologic modeling of a perennial firn aquifer in southeast Greenland. *Journal of Glaciology*, 1–16 (doi: 10.1017/jog.2022.88)

Miller OL, Solomon DK, Miège C, Koenig LS, Forster RR, Montgomery LN, Schmerr N, Ligtenberg SRM, Legchenko A and Brucker L (2017) Hydraulic conductivity of a firn aquifer in southeast Greenland. *Frontiers in Earth Science*, **5**(38) (doi: 10.3389/feart.2017.00038)

Mouginot J, Rignot E, Bjørk AA, van den Broeke M, Millan R, Morlighem M, Noël B, Scheuchl B and Wood M (2019) Forty-six years of greenland ice sheet mass balance from 1972 to 2018. *Proceedings of the National Academy of Sciences*, **116**(19), 9239–9244 (doi: 10.1073/pnas.1904242116)

Müller F (1962) Zonation in the accumulation area of the glaciers of Axel Heiberg Island, N.W.T., Canada. *Journal of Glaciology*, **4**(33), 302–311 (doi: 10.3189/s0022143000027623)

Nghiem SV, Hall DK, Mote TL, Tedesco M, Albert MR, Keegan K, Shuman CA, DiGirolamo NE and Neumann G (2012) The extreme melt across the greenland ice sheet in 2012. *Geophysical Research Letters*, **39**(20), L20502 (doi: 10.1029/2012gl053611)

Nienow PW, Sole AJ, Slater DA and Cowton TR (2017) Recent advances in our understanding of the role of meltwater in the greenland ice sheet system. *Current Climate Change Reports*, **3**(4), 330–344 (doi: 10.1007/s40641-017-0083-9)

Noël B, van de Berg WJ, van Wessem JM, van Meijgaard E, van As D, Lenaerts JTM, Lhermitte S, Kuipers Munneke P, Smeets CJPP, van Ulft LH, van de Wal RSW and van den Broeke MR (2018) Modelling the climate and surface mass balance of polar ice sheets using RACMO2 – part 1: Greenland (1958–2016). *The Cryosphere*, **12**(3), 811–831 (doi: 10.5194/tc-12-811-2018)

Noël B, van de Berg WJ, Lhermitte S and van den Broeke MR (2019) Rapid ablation zone expansion amplifies north greenland mass loss. *Science Advances*, **5**(9), eaaw0123 (doi: 10.1126/sciadv.aaw0123)

Obleitner F and Lehning M (2004) Measurement and simulation of snow and superimposed ice at the kongsvegen glacier, svalbard (spitzbergen). *Journal of Geophysical Research: Atmospheres*, **109**(D4) (doi: 10.1029/2003jd003945)

Parry V, Nienow P, Mair D, Scott J, Hubbard B, Steffen K and Wingham D (2007) Investigations of meltwater refreezing and density variations in the snowpack and firn within the percolation zone of the greenland ice sheet. *Annals of Glaciology*, **46**, 61–68 (doi: 10.3189/172756407782871332)

Pfeffer WT and Humphrey NF (1998) Formation of ice layers by infiltration and refreezing of meltwater. *Annals of Glaciology*, **26**, 83–91 (doi: 10.3189/1998aog26-1-83-91)

Pfeffer WT, Meier MF and Illangasekare TH (1991) Retention of greenland runoff by refreezing: Implications for projected future sea level change. *Journal of Geophysical Research*, **96**(C12), 22117 (doi: 10.1029/91jc02502)

Porter C, Morin P, Howat I, Noh MJ, Bates B, Peterman K, Keesey S, Schlenk M, Gardiner J, Tomko K, Willis M, Kelleher C, Cloutier M, Husby E, Foga S, Nakamura H, Platson M, Wethington M, Williamson C, Bauer G, Enos J, Arnold G, Kramer W, Becker P, Doshi A, D'Souza C, Cummens P, Laurier F and Bojesen M (2018) "arcticdem", harvard dataverse, v1 (doi: 10.7910/DVN/OHHUKH)

Reeh N (1991) Parameterization melt rate and surface temperature on the Greenland ice sheet. *Polarforschung*, **59**, 113–128

Rennermalm ÅK, Hock R, Covi F, Xiao J, Corti G, Kingslake J, Leidman SZ, Miège C, Macferrin M, Machguth H, Osterberg E, Kameda T and McConnell J (2021) Shallow firn cores 1989–2019 in southwest Greenland's percolation zone reveal decreasing density and ice layer thickness after 2012. *Journal of Glaciology*, 1–12 (doi: 10.1017/jog.2021.102)

Samaniego L, Kumar R and Attinger S (2010) Multiscale parameter regionalization of a grid-based hydrologic model at the mesoscale. *Water Resources Research*, **46**(5) (doi: 10.1029/2008wr007327)

Shumskii P (1964) *Principles of structural glaciology*. Dover Publications, New York

Smeets PCJP, Munneke PK, van As D, van den Broeke MR, Boot W, Oerlemans H, Snellen H, Reijmer CH and van de Wal RSW (2018) The k-transect in west greenland: Automatic weather station data (1993–2016). *Arctic, Antarctic, and Alpine Research*, **50**(1) (doi: 10.1080/15230430.2017.1420954)

Smith LC, Yang K, Pitcher LH, Overstreet BT, Chu VW, Rennermalm ÅK, Ryan JC, Cooper MG, Gleason CJ, Tedesco M, Jeyaratnam J, van As D, van den Broeke MR, van de Berg WJ, Noël B, Langen PL, Cullather RI, Zhao B, Willis MJ, Hubbard A, Box JE, Jenner BA and Behar AE (2017) Direct measurements of meltwater runoff on the greenland ice sheet surface. *Proceedings of the National Academy of Sciences*, **114**(50), E10622–E10631 (doi: 10.1073/pnas.1707743114)

Steger CR, Reijmer CH, van den Broeke MR, Wever N, Forster RR, Koenig LS, Munneke PK, Lehning M, Lhermitte S, Ligtenberg SRM, Miège C and Noël BPY (2017) Firn meltwater retention on the greenland ice sheet: A model comparison. *Frontiers in Earth Science*, **5**, 1–16 (doi: 10.3389/feart.2017.00003)

Stevens IT, Irvine-Fynn TD, Porter PR, Cook JM, Edwards A, Smart M, Moorman BJ, Hodson AJ and Mitchell AC (2018) Near-surface hydraulic conductivity of northern hemisphere glaciers. *Hydrological Processes*, **32**(7), 850–865 (doi: 10.1002/hyp.11439)

Tedesco M and Fettweis X (2020) Unprecedented atmospheric conditions (1948–2019) drive the 2019 exceptional melting season over the greenland ice sheet. *The Cryosphere*, **14**(4), 1209–1223 (doi: 10.5194/tc-14-1209-2020)

Tedstone A and Machguth H (2022) Increasing surface runoff from greenland's firn areas. *Nature Climate Change* (doi: 10.1038/s41558-022-01371-z) the IMBIE Team (2019) Mass balance of the greenland ice sheet from 1992 to 2018. *Nature*, **579**(7798), 233–239 (doi: 10.1038/s41586-019-1855-2)

van As D (2011) Warming, glacier melt and surface energy budget from weather station observations in the melville bay region of northwest greenland. *Journal of Glaciology*, **57**(202), 208–220 (doi: 10.3189/002214311796405898)

van As D, Hubbard AL, Hasholt B, Mikkelsen AB, van den Broeke MR and Fausto RS (2012) Large surface meltwater discharge from the kangerlussuaq sector of the greenland ice sheet during the record-warm year 2010 explained by detailed energy balance observations. *The Cryosphere*, **6**(1), 199–209 (doi: 10.5194/tc-6-199-2012)

van As D, Box JE and Fausto RS (2016) Challenges of quantifying meltwater retention in snow and firn: An expert elicitation. *Frontiers in Earth Science*, **4**(101) (doi: 10.3389/feart.2016.00101)

van As D, Mikkelsen AB, Nielsen MH, Box J, Liljedahl LC, Lindbäck K, Pitcher L and Hasholt B (2017) Hypsometric amplification and routing moderation of Greenland ice sheet meltwater release. *The Cryosphere*, **11**, 1371–1386 (doi: 10.5194/tc-11-1371-2017)

van de Wal R, Greuell W, van den Broeke M, Reijmer C and Oerlemans J (2005) Surface mass-balance observations and automatic weather station data along a transect near kangerlussuaq, west greenland. *Annals of Glaciology*, **42**, 311–316 (doi: 10.3189/172756405781812529)

van de Wal RSW, Boot W, Smeets CJPP, Snellen H, van den Broeke MR and Oerlemans J (2012) Twenty-one years of mass balance observations along the k-transect, west greenland. *Earth System Science Data*, **4**(1), 31–35 (doi: 10.5194/essd-4-31-2012)

van den Broeke M, Enderlin E, Howat I, Kuipers Munneke P, Noël B, van de Berg WJ, van Meijgaard E and Wouters B (2016) On the recent contribution of the Greenland ice sheet to sea level change. *The Cryosphere*, **10**, 1933–1946 (doi: 10.5194/tc-10-1933-2016)

van den Broeke M, Box J, Fettweis X, Hanna E, Noël B, Tedesco M, van As D, van de Berg WJ and van Kampenhout L (2017) Greenland ice sheet surface mass loss: Recent developments in observation and modeling. *Current Climate Change Reports*, **3**(4), 345–356 (doi: 10.1007/s40641-017-0084-8)

Vandecrux B, Mottram R, Langen PL, Fausto RS, Olesen M, Stevens CM, Verjans V, Leeson A, Ligtenberg S, Munneke PK, Marchenko S, van Pelt W, Meyer CR, Simonsen SB, Heilig A, Samimi S, Marshall S, Machguth H, MacFerrin M, Niwano M, Miller O, Voss CI and Box JE (2020) The firn meltwater retention model intercomparison project (RetMIP): evaluation of nine firn models at four weather station sites on the greenland ice sheet. *The Cryosphere*, **14**(11), 3785–3810 (doi: 10.5194/tc-14-3785-2020)

Xiao J, Rennermalm ÅK, Covi F, Hock R, Leidman SZ, Miège C, MacFerrin MJ and Samimi S (2022) Local-scale spatial variability in firn properties in southwest greenland. *Frontiers in Earth Science*, **10** (doi: 10.3389/feart.2022.938246)

Zuo Z and Oerlemans J (1996) Modelling albedo and specific balance of the greenland ice sheet: calculations for the søndre strømfjord transect. *Journal of Glaciology*, **42**(141), 305–317 (doi: 10.3189/s0022143000004160)